Suppressed monocyte recruitment drives macrophage removal from atherosclerotic plaques of *Apoe*$^{-/-}$ mice during disease regression

Stephane Potteaux,[1] Emmanuel L. Gautier,[1] Susan B. Hutchison,[1] Nico van Rooijen,[2] Daniel J. Rader,[3] Michael J. Thomas,[4] Mary G. Sorci-Thomas,[5] and Gwendalyn J. Randolph[1]

[1]Department of Gene and Cell Medicine and Immunology Institute, Mount Sinai School of Medicine, New York, New York, USA. [2]Department of Molecular Cell Biology, Free University Medical Center, Amsterdam, The Netherlands. [3]University of Pennsylvania School of Medicine, Philadelphia, Pennsylvania, USA. [4]Department of Biochemistry and [5]Department of Pathology, Wake Forest University School of Medicine, Winston-Salem, North Carolina, USA.

Experimental models of atherosclerosis suggest that recruitment of monocytes into plaques drives the progression of this chronic inflammatory condition. Cholesterol-lowering therapy leads to plaque stabilization or regression in human atherosclerosis, characterized by reduced macrophage content, but the mechanisms that underlie this reduction are incompletely understood. Mice lacking the gene *Apoe* (*Apoe*$^{-/-}$ mice) have high levels of cholesterol and spontaneously develop atherosclerotic lesions. Here, we treated *Apoe*$^{-/-}$ mice with apoE-encoding adenoviral vectors that induce plaque regression, and investigated whether macrophage removal from plaques during this regression resulted from quantitative alterations in the ability of monocytes to either enter or exit plaques. Within 2 days after apoE complementation, plasma cholesterol was normalized to wild-type levels, and HDL levels were increased 4-fold. Oil red O staining and quantitative mass spectroscopy revealed that esterified cholesterol content was markedly reduced. Plaque macrophage content decreased gradually and was 72% lower than baseline 4 weeks after apoE complementation. Importantly, this reduction in macrophages did not involve migratory egress from plaques or CCR7, a mediator of leukocyte emigration. Instead, marked suppression of monocyte recruitment coupled with a stable rate of apoptosis accounted for loss of plaque macrophages. These data suggest that therapies to inhibit monocyte recruitment to plaques may constitute a more viable strategy to reduce plaque macrophage burden than attempts to promote migratory egress.

Introduction

Atherosclerosis is a chronic inflammatory disease of the arterial wall that is currently the major cause of death in developed countries. The disease develops slowly and silently over decades, progressively evolving from fatty streaks characterized mainly by monocyte-derived cells filled with cholesterol esters to advanced plaques with more complex cellular composition, lipid pools filled with necrotic debris, and calcified material (1). Experiments in mouse models of atherosclerosis reveal that recruitment of monocytes into plaques drives disease progression (2). Overall, the inflammatory mechanisms of plaque formation have been extensively described, whereas mechanisms that reverse disease are less well understood. Vulnerable plaques are characterized by substantial necrotic core, reduced fibrous cap thickness, and fibrous cap inflammation wherein activated macrophages and dendritic cells along with associated T cells are invariably found to localize to sites of plaque rupture (3–7). Conversely, plaque stabilization is associated with a diminution in plaque macrophage content and a replacement of these cells with collagenous matrix. However, the cellular and molecular mechanisms underlying the process by which macrophages are removed from plaques during lipid-lowering therapy have not been determined. If these mechanisms were known, therapies to reinforce events that promote macrophage removal would likely improve clinical success in reducing further critical cardiovascular events.

Accumulation of monocyte-derived cells in atherosclerotic plaques is understood to be the result of several processes. Monocyte recruitment to plaques in mouse models of atherosclerosis occurs throughout different stages of plaque progression, and the rate of recruitment is increased when mice are maintained on a high-fat, cholesterol-enriched diet (8, 9). The potential for monocytes to be recruited into plaques from the blood is strongly affected by monocyte frequency in the circulation (10), implying that the availability of monocytes in the circulation may be rate limiting to atherosclerosis progression. Accordingly, monocytosis is an independent risk factor for atherosclerosis progression in humans (11–14).

Besides recruitment, survival and/or proliferation of monocyte-derived cells in plaques could affect overall macrophage accumulation. Recent studies indicate that intimal cell proliferation increases with hypercholesterolemia in early lesions (15) and correlates with plaque complexity in advanced lesions (16). Furthermore, the 9p21 genetic locus, which impacts proliferation of vascular cells, has been associated with susceptibility to coronary artery disease (17–19). With regard to survival, apoptosis of macrophages in the plaque is detected at all stages of the disease and is not proinflammatory in early, fatty streak lesions (20, 21). Mutations in *Cx3cr1* and *Csf1* accelerate loss of macrophages from plaques, at least in

Conflict of interest: The authors have declared that no conflict of interest exists.
Citation for this article: *J Clin Invest.* 2011;121(5):2025–2036. doi:10.1172/JCI43802.

part through increased apoptosis (2, 22). In later stages of disease, clearance of apoptotic cells (also called efferocytosis) becomes compromised (21). As a consequence of decreased efferocytosis, apoptosis leads to secondary necrosis. In this setting, accumulation of dead cell debris amplifies proinflammatory signals and triggers further monocyte recruitment (20).

Finally, accumulation of monocyte-derived cells in the plaque may also result from their inability to leave plaque. Macrophages are normally removed from sites of resolving inflammation by migration through lymphatics to lymph nodes (23). Furthermore, in a surgical model of plaque regression in which plaque-bearing aortae are transplanted into wild-type mice with low levels of circulating cholesterol, rapid removal of plaque foam cells correlates with the onset of their emigration to lymph nodes (24). Further, this migration appears to depend upon the chemotactic ligands of the G protein–coupled receptor CCR7 (25). It has been proposed that unloading of cholesterol by plaque macrophages may restore emigration from plaques (26), consistent with the concept that cholesterol has a direct negative effect on the motility of macrophages (27).

In this study, we set out to investigate the cellular mechanism(s) that quantitatively account for macrophage removal from plaques in response to aggressive lipid lowering. Based on our earlier observations in a surgical model of plaque regression (24, 26), we predicted that emigration of monocyte-derived cells would be a major feature of macrophage removal from plaques. However, our earlier studies did not determine whether migratory egress was a minor or major aspect of macrophage removal from a quantitative perspective. Moreover, the requirement for re-anastomosis of lymphatics in the adventitia may render data from the surgical model difficult to translate to settings wherein surgical intervention and lymphatic remodeling is not a feature. Thus, the present study was designed to quantitatively determine the extent to which changes in the rate of monocyte recruitment, apoptosis, or migratory egress account for plaque macrophage removal from plaques. We focused on a model system in which surgery is not required and instead studied the mechanism of macrophage removal from plaques of *Apoe*$^{-/-}$ mice treated with a viral vector encoding apoE (28). This treatment lowers total cholesterol in plasma while raising HDL (28). In turn, plaques regress, and foam cell loss from plaques is substantial (28). Here, we show that in concert with a marked reduction in plaque cholesterol esters, plaque macrophage content in *Apoe*$^{-/-}$ mice declined by more than 70% in the course of the weeks following apoE complementation. The diminution in plaque macrophages did not result from migratory egress, as we had hypothesized, and did not require CCR7. Instead, loss of plaque macrophages resulted from greatly attenuated recruitment of new circulating monocytes. This decreased recruitment was associated with a reduced expression of inflammatory and adhesion molecules in the circulating monocytes and in the vascular wall. These findings bolster the rationale for developing therapies to target inhibition of monocyte recruitment in order to reduce macrophage burden in advanced atherosclerotic plaques.

Results

Reduction in lesional macrophage content is preceded by de-esterification of cholesterol within plaques. Treatment of *Apoe*$^{-/-}$ mice with viral vectors encoding apoE (ad-hApoE3) causes lesion regression characterized by loss of oil red O (ORO) staining (to identify neutral lipids) and macrophages from plaques (28), but the kinetics by which changes occur in *Apoe*$^{-/-}$ plaques following apoE complementation have not been reported. Thus, we analyzed the course of changes observed from 2 days to 1, 2, 4, or 6 weeks after treatment of high-fat diet–fed (HFD-fed) *Apoe*$^{-/-}$ mice with ad-hApoE3, employing empty adenoviral vector (ad-Empty) as a control of plaque progression. Total cholesterol decreased from approximately 1,000 mg/dl to 100 mg/dl within 2 days following infection with ad-hApoE3 vector, and remained low for up to 6 weeks (Figure 1, A and B, and data not shown). Within 2 days, HDL was elevated more than 4-fold and continued to rise, reaching a plateau by day 7 (Figure 1B). Plaque area in the aortic sinus (Figure 1C) and aortic arch (data not shown) increased by 4 weeks in control ad-Empty vector–treated mice, whereas plaque area was stabilized in ad-hApoE3–treated animals, showing no changes in relation to a baseline cohort euthanized at the time when vector treatment began (Figure 1C and data not shown). In a separate experiment wherein *Apoe*$^{-/-}$ mice were euthanized 6 weeks after vector treatment, ad-hApoE3 vector reduced plaque area and stenosis relative to baseline (Supplemental Figure 1; supplemental material available online with this article; doi:10.1172/JCI43802DS1), consistent with past evidence indicating that over many weeks, regression of plaque area occurs (28).

We next quantified macrophage area in plaques as a function of treatment with ad-hApoE3 or ad-Empty vector. CD68$^+$ macrophages disappeared in a linear fashion from plaques over the weeks following treatment with ad-hApoE3 vector (Figure 1D) in contrast to the ad-Empty group, where they increased substantially over time (Figure 1D). However, the reduction in macrophage content only became statistically significant 4 weeks after ad-hApoE3 treatment (Figure 1, D and E), when it was reduced by an average of 72%. The marked loss of macrophages in the ad-hApoE3–treated group was further confirmed by staining for other macrophage markers, F4/80 and MOMA-2 (Supplemental Figure 2, A and B). Accompanying the decrease in macrophage content in plaques of ad-hApoE3–infected mice, we observed increased collagen accumulation, as analyzed with Sirius red staining (Supplemental Figure 2C), and conserved smooth muscle cell content, as revealed by α-actin staining (Supplemental Figure 2D).

To document how changes in plaque cholesterol distribution and mass correlated with the decrease in circulating cholesterol or plaque macrophages observed in ad-hApoE3–treated mice, we first stained plaque sections with ORO and then quantified total, free, and esterified cholesterol using mass spectroscopy (29). ORO$^+$ area did not change in ad-Empty vector–treated mice over time. By contrast, in ad-hApoE3 vector–treated mice, ORO$^+$ area in the plaque was decreased by more than one-half (Figure 1F and Supplemental Figure 3A), and also showed substantial reduction in other tissues, such as the liver, 4 weeks after infection (Supplemental Figure 3B). We verified that the adenovirus infection had no detrimental effect on liver function by assessing alanine transaminase (ALT) activity in plasma at different time points (Supplemental Figure 3C). By 4 weeks after infection, ALT levels approached baseline in all groups (Supplemental Figure 3C). Nevertheless, we noted a transient effect of ad-hApoE3 on day 7 (Supplemental Figure 3C). The specific and prominent increase in ALT on day 7 after ad-hApoE3 infection was paralleled with a peak of large cholesterol-rich HDL particles (big HDL) accumulation in the plasma (Figure 1B), consistent with the possibility that mobilization of cholesterol to the liver peaks around day 7 and transiently affects liver metabolism. This finding is reminiscent of a previous study on virally induced DGAT1 overexpression, where a similar outcome was observed (30).

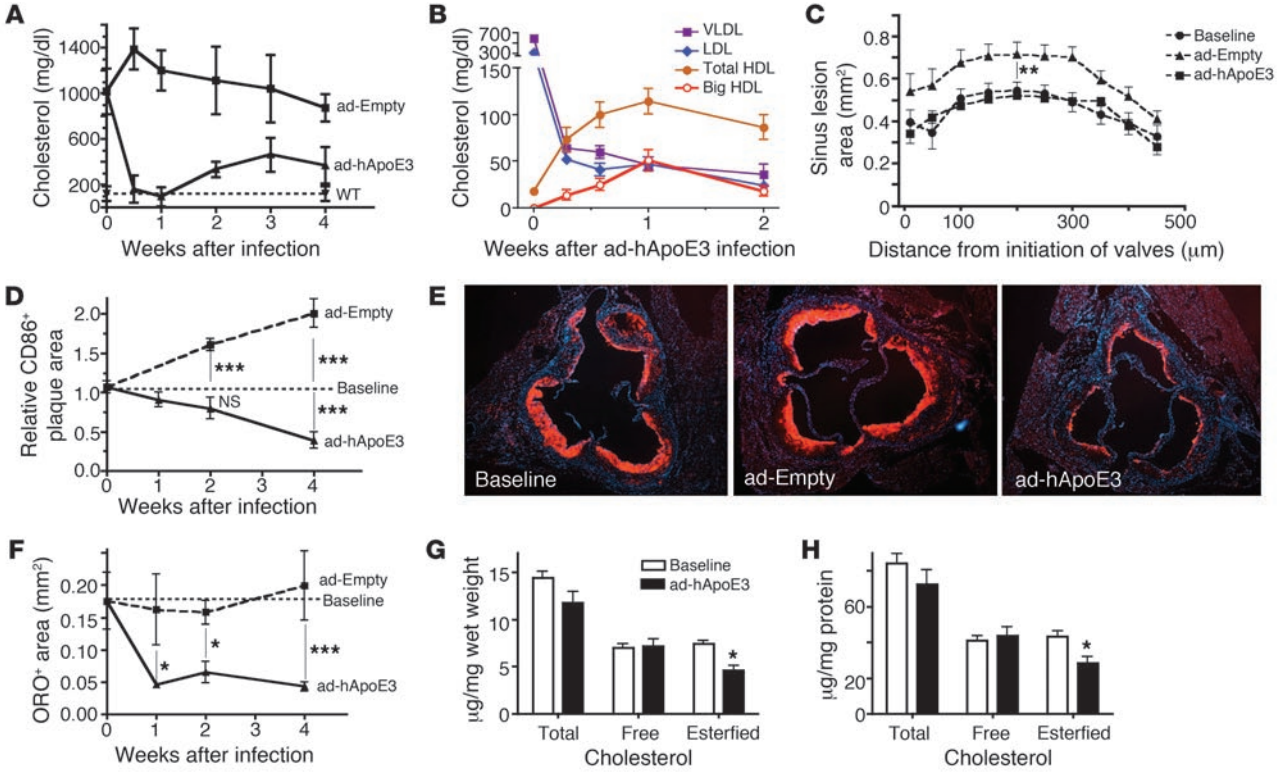

Figure 1

Kinetics of changes within *Apoe*$^{-/-}$ plaques following apoE complementation. *Apoe*$^{-/-}$ mice were fed a HFD for 9 weeks before establishment of a baseline group or starting treatment with ad-hApoE3 or ad-Empty vector. The evolution of changes within plaque after 1, 2, or 4 weeks following adenoviral infection was characterized. (**A**) Total cholesterol measurements. Dashed line depicts the values obtained from age- and sex-matched C57BL/6 *Apoe*$^{+/+}$ mice. (**B**) The plasma lipoprotein profile as a function of time following apoE complementation. (**C**) Lesion area was measured on 8-μm sections at 48-μm intervals, starting from the initiation of valves. (**D**) Macrophage area was quantified by CD68^{+} area and normalized to the average CD68^{+} area from the corresponding baseline group lesions. (**E**) Representative photomicrographs of CD68^{+} staining in sections of the aortic sinus of each experimental group. Red, CD68; blue, DAPI. Original magnification, ×50. (**F**) Neutral lipid area within lesions was quantified by ORO staining within each treatment group over time; the dashed line refers to baseline values obtained in *Apoe*$^{-/-}$ mice after 9 weeks of HFD feeding. (**G** and **H**) Total, free, and esterified cholesterol mass analysis at baseline or 14 days after apoE complementation normalized to wet weight of tissue (**G**) or tissue protein content (**H**) from 7–8 mice per group. Data represent mean ± SEM, except in **A**, which depicts mean ± SD. $^{*}P < 0.05$, $^{**}P < 0.01$, $^{***}P < 0.001$. Results are compiled from 3 independent experiments with 5–8 animals per group per experiment.

Given the impressive reduction in ORO^{+} area within plaques, we set out to quantify the changes in aortic cholesterol mass. Cholesterol ester mass dropped substantially, by one-third (Figure 1G), whereas the clear trend downward in total cholesterol mass did not reach statistical significance (Figure 1G). These data corresponded to an increased ratio of free cholesterol to total cholesterol within the aorta in response to apoE complementation (49% ± 3% to 61% ± 4%, before versus after apoE complementation), indicating that the proportion of cholesterol present in esterified form was decreased (51% ± 3% to 39% ± 4%, before versus after apoE complementation). These results are consistent with our ORO staining analyses (Figure 1F), as ORO staining detects only esterified cholesterol (31). Putting these observations together, we observe that an initial reduction in plasma cholesterol and increase in circulating HDL were rather rapidly followed by reduced cholesterol ester–laden macrophages in plaque. The reduction in cholesterol ester–laden foam cell content occurred prior to, rather than concomitantly with, the loss of plaque macrophages.

Reduction in plaque macrophages does not depend upon CCR7 or migratory egress of cells. We next set out to determine how the decrease in macrophage content within plaques was achieved. Given our past findings in the surgical model of regression, we hypothesized that monocyte-derived cell disappearance would be a consequence of their emigration out of plaque, through mobilization into adventitial lymphatics (24). Accordingly, we anticipated that deficiency in CCR7, a key mediator in leukocyte emigration through lymphatics (32–34) and a proposed modulator of regression in the surgical model (25), would prevent loss of plaque macrophages in response to ad-hApoE3 treatment. We thus crossed *Apoe*$^{-/-}$ mice with *Ccr7*$^{-/-}$ mice to generate *Apoe*$^{-/-}$*Ccr7*$^{-/-}$ double-knockout mice and analyzed the evolution of macrophage area within plaques after ad-hApoE3 infection. The absence of CCR7 and ApoE led to increased levels of circulating leukocytes and decreased lymphocyte and dendritic cell accumulation in the lymph nodes similar to the CCR7 single knockout (32, 33) (data not shown). However, after 9 weeks of HFD feeding (14–15 weeks of age), atherosclerotic plaques of *Apoe*$^{-/-}$*Ccr7*$^{-/-}$ mice showed no significant difference in size or in macrophage content compared with *Apoe*$^{-/-}$*Ccr7*$^{+/+}$ control littermates, although trends toward somewhat smaller lesions in the absence of CCR7 were observed (Figure 2, A and B). In contrast to expectations gen-

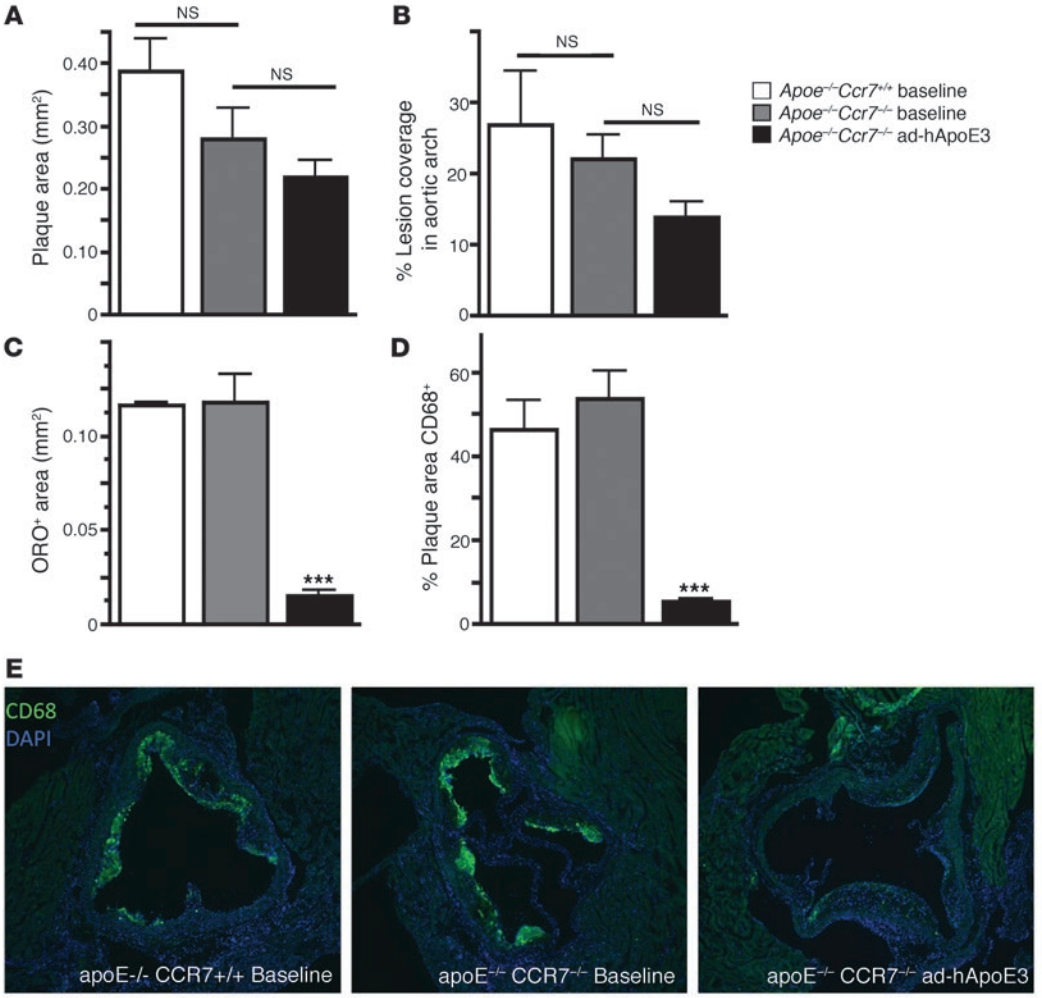

Figure 2

CCR7-independent removal of *Apoe*$^{-/-}$ plaque macrophages after apoE complementation. *Apoe*$^{-/-}$*Ccr7*$^{-/-}$ and *Apoe*$^{-/-}$*Ccr7*$^{+/+}$ (littermate control) mice were fed HFD for 9 weeks. A cohort of animals from each genotype was sacrificed to establish baseline (white and gray bars). A second cohort of *Apoe*$^{-/-}$*Ccr7*$^{-/-}$ was then infected with ad-hApoE3 vector for 4 weeks (black bar) before sacrifice. (**A**) Plaque area was quantified in aortic sinus sections and (**B**) en face aortic arch preparation. (**C**) Lipid area was measured by ORO coloration and (**D**) macrophage content by CD68^{+}staining. (**E**) Representative photomicrographs of macrophage (CD68^{+}) area in sections of the aortic sinus at time of sacrifice in each group. Green, CD68; blue, DAPI. Original magnification, ×50. Data represent mean ± SEM from 2 independent experiments; n = 3 mice in *Apoe*$^{-/-}$*Ccr7*$^{+/+}$ baseline group, n = 5 in *Apoe*$^{-/-}$*Ccr7*$^{-/-}$ baseline group, n = 6 in *Apoe*$^{-/-}$*Ccr7*$^{-/-}$ ad-hApoE3 group; ***P < 0.001.

erated from observations in the surgical model of regression (25), lipid and macrophage loss from plaques of *Apoe*$^{-/-}$*Ccr7*$^{-/-}$ mice was massive after treatment with the ad-hApoE3 vector (Figure 2, C and D), thus illustrating that CCR7 is not necessary for profound loss of lipid or macrophages from plaques.

To more generally address the importance of migratory egress from plaques as a means of removing macrophages during plaque regression, which may occur in a CCR7-independent manner, we employed a modified version of the phagocyte-tracking approach previously developed in our laboratory (9, 35). This technique independently labels about 10%–20% of the two endogenous subsets of monocytes in the circulation and is useful in monitoring and quantifying monocyte subset entry into (9) and egress from plaques (36). Over time, if latex bead^{+} monocyte-derived cells die or exocytose beads, the beads will not disappear, as they are non-degradable and are too large to cross the endothelial barrier passively, but may instead label other phagocytes within the plaque. In past studies, we have documented that latex bead transfer from phagocyte to phagocyte can occur (37) and that emigration of bead-labeled monocyte-derived cells is not impeded (9, 38, 39). Once peak accumulation of latex bead^{+} monocytes occurs in plaques, if thereafter some monocyte-derived cells migrate out of lesions, then the total number of bead^{+} cells in the lesions will decrease. On the other hand, if there is no emigration of monocyte-derived cells out of lesions, the bead frequency within plaques will remain constant.

To verify that this method can track emigration from plaques, we first tested it using the surgical model of regression, wherein migratory egress from mouse plaques was initially described (24). We labeled blood monocytes with beads and then harvested aortic

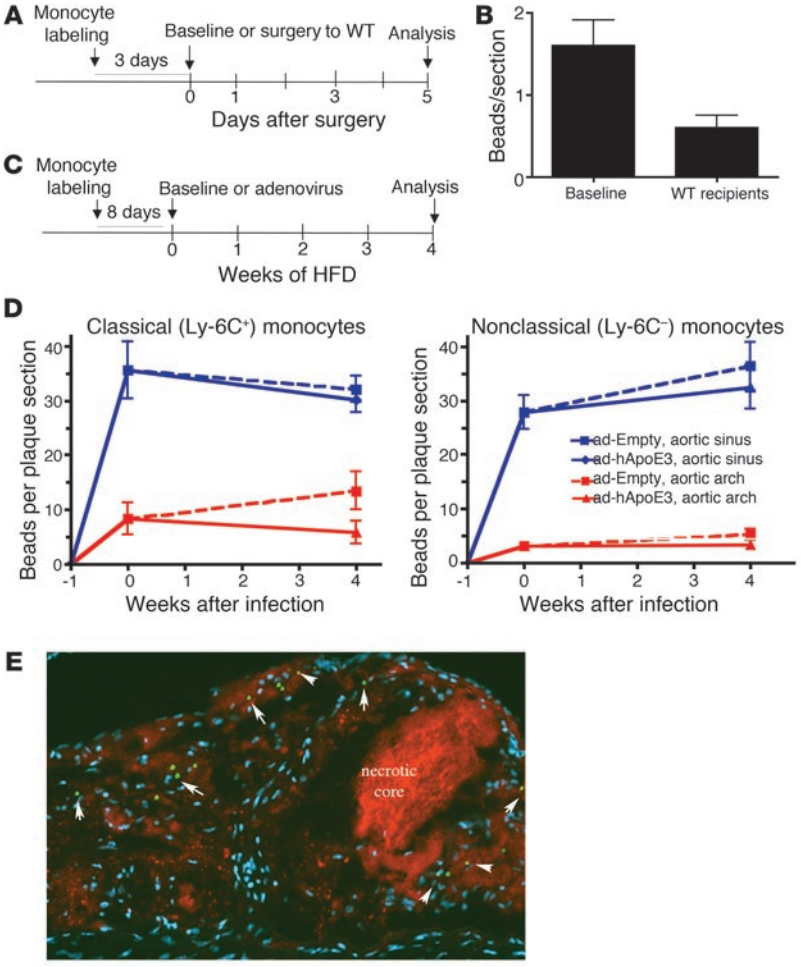

Figure 3
Analysis of migratory egress from atherosclerotic plaques in *Apoe*$^{-/-}$ mice following apoE complementation. (**A**) Diagram depicts experimental design in which the Ly-6C^{lo} monocytes of mice were labeled with beads in the blood before the mice served as transplant donors in a surgical model of regression. (**B**) Quantification of the number of beads per cross section of the aortic arch before (baseline) and after plaque regression in WT transplant recipients. Data were pooled from 3 independent experiments; $n = 5$ in the baseline group, $n = 7$ in the WT recipient group. Difference from baseline is significant, $P < 0.01$. (**C**) Experimental design to study migratory egress from plaques of *Apoe*$^{-/-}$ mice after apoE complementation. (**D**) Quantification of bead number in aortic sinus plaques (blue lines) or aortic arch (lesser curvature; red lines) after Ly-6C^{hi} (upper graph; $n = 5$–7 mice per data point) or Ly-6C^{lo} (lower graph; $n = 10$–16 mice per data point) monocytes were initially labeled in the blood. (**E**) Microphotograph of beads (green particles, some indicated by arrows) localized within an aortic arch plaque 4 weeks after labeling in the control group. Non-overlapping ORO (red) and DAPI (blue) staining reveals necrotic core. Data represent mean ± SEM.

arches from these animals after 3 days. A subset of aortic arches was used to quantify baseline recruitment, while the others were transplanted into wild-type C57BL/6 mice (*Apoe*$^{+/+}$) to allow plaque regression. Mice receiving these aortic transplants were sacrificed 5 days later (Figure 3A). We then quantified the number of beads per 6-μm section of the lesser curvature of the aortic arch, comparing the number of beads per section at baseline prior to surgery to the number of beads per section 5 days after surgery. A 63% decline in bead content was observed at the post-transplantation end point (Figure 3B). Thus, in the surgical model of regression, monocyte-derived cell emigration from the intima indeed occurred, and the process appeared quantitatively significant enough to mediate loss of macrophages that accompanies regression. Furthermore, these data serve as a proof of concept that beads within plaques can be removed under conditions of phagocyte mobilization.

To monitor migratory egress from *Apoe*$^{-/-}$ plaques after apoE complementation, we labeled circulating monocytes in *Apoe*$^{-/-}$ mice with latex beads and tracked the persistence of this label in plaques as a function of ad-hApoE3 or ad-Empty vector treatment (Figure 3C). We set up two parallel studies wherein we independently labeled the classical (Ly-6C^{hi}) and nonclassical (Ly-6C^{lo}) subsets of monocytes as the populations to carry latex beads into plaques (2, 9). Mice were housed without further manipulation for the next 8 days to permit accumulation of bead^{+} monocytes in the plaques. Within this period, 73% of bead^{+} monocytes were cleared from the blood due to recruitment into tissues and normal turnover (Supplemental Figure 4). At day 8, we sacrificed one-third of the mice for baseline analysis of plaque area, lipid and macrophage content, and number of beads per plaque section. Other similarly bead-labeled mice were infected with ad-hApoE3 or ad-Empty vector 8 days after monocyte labeling and sacrificed at 4 weeks after adenoviral infection. Bead number was quantified in the aortic sinus and the lesser curvature for comparison to the number of bead^{+} cells in analogous sections obtained at baseline.

From the baseline data obtained in aortic sinus, we observed that, in contrast to previous studies in the aortic arch (9), labeled Ly-6C^{hi} monocytes did not outnumber labeled Ly-6C^{lo} monocytes in entering aortic sinus plaque (Figure 3D), where robust recruitment of both monocytes was apparent. To analyze migratory egress from plaques, accumulation of bead^{+} monocytes at the experimental end point was compared with that in the baseline group. The number of beads per plaque section in *Apoe*$^{-/-}$ mice treated with ad-Empty for 4 weeks after baseline monocyte entry was the same as observed at baseline. This result was true whether circulating classical Ly-6C^{hi} or nonclassical Ly-6C^{lo} monocytes were initially labeled or whether the aortic sinus or lesser curvature of the aorta was examined (Figure 3D). In agreement with previous findings (24), this result suggests that migratory egress of plaque phagocytes is rare or does not occur in conditions of plaque progression. Unexpectedly, we did not observe any diminution in bead labeling

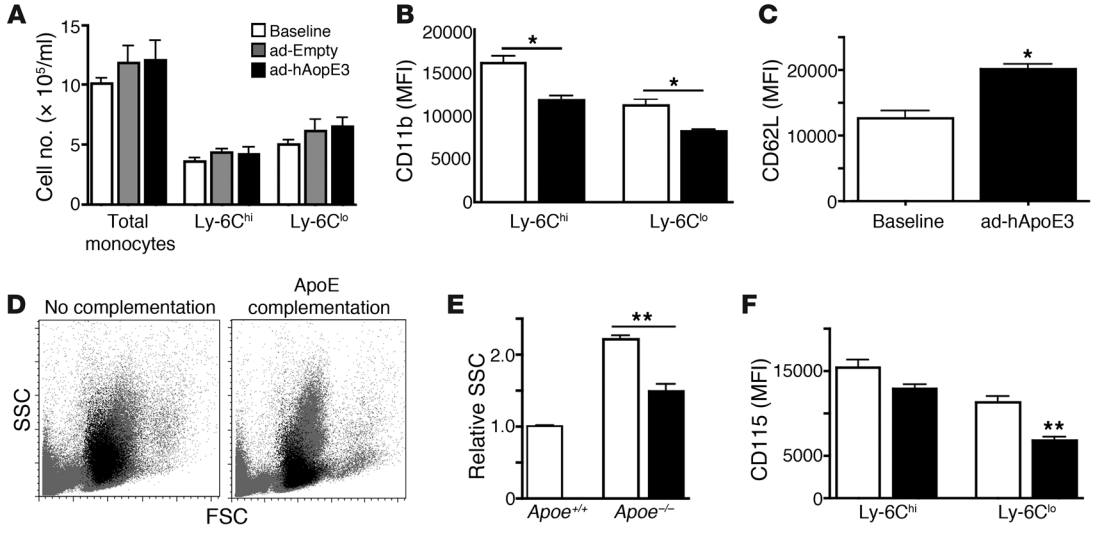

Figure 4
Analysis of blood monocyte numbers and phenotype following apoE complementation. (**A**) Total monocytes and monocyte subsets were quantified by flow cytometry in blood of baseline mice or 4 weeks after infection with ad-Empty and ad-hApoE3 (n = 10–34 mice per bar). (**B**) CD11b and (**C**) CD62L (Ly-6C^{hi} monocytes only) expression was analyzed with (black bars) or without apoE complementation (white bars) of *Apoe*$^{-/-}$ mice maintained on a HFD. n = 5–9 mice per bar; *P < 0.01. (**D**) Flow plot overlays show whole leukocyte fraction in blood (gray) overlaid with profiles of Ly-6C^{lo} monocytes (black) from *Apoe*$^{-/-}$ mice fed a HFD followed by apoE complementation or no complementation. (**E**) Summary of relative changes in SSC-A shifts in Ly-6C^{lo} monocytes from *Apoe*$^{-/-}$ mice on a HFD complemented (black bar) or not (white bars) with apoE-encoding vector. Data are compared with SSC-A of monocytes from *Apoe*$^{+/+}$ control mice. (**F**) Effect of hApoE3 complementation on surface expression of CD115. n = 5 mice per bar; **P < 0.001.

in *Apoe*$^{-/-}$ mice treated with ad-hApoE3 (Figure 3, D and E), even though (as shown in Figure 1) macrophage loss from plaque was significant under these conditions. This lack of bead removal from plaques was not because the label was sequestered outside of macrophages, as even at late time points, very few beads were present in necrotic core or outside of macrophages (Figure 3E and data not shown). Overall, our analyses failed to support the hypothesis that migratory egress is responsible for the marked removal of macrophages that characterizes ad-hApoE3–treated *Apoe*$^{-/-}$ mice.

Markedly inhibited infiltration of both monocyte subsets into plaque mediates macrophage loss from plaques. Without experimental support for a role of migratory egress in mediating removal of macrophages from *Apoe*$^{-/-}$ plaques after apoE complementation, we initiated studies to determine whether monocyte recruitment was altered. Since hypercholesterolemia increases monocytes in the circulation, making more monocytes available for recruitment into plaques (9, 40), we first examined whether ad-hApoE3 or ad-Empty vector treatment influenced monocyte counts or subset frequency in the blood. Blood monocyte subsets were discriminated by flow cytometry, based on their expression of CD115 and Ly-6C (9). Neither ad-hApoE3 nor ad-Empty virus significantly influenced monocyte numbers of either circulating subset (Figure 4A), indicating that the loss of macrophages observed in plaques of ad-hApoE3–treated mice was not downstream of a notable decrease in blood monocyte counts. However, monocytes in the circulation altered their phenotype. Monocytes from ad-hApoE3 vector–treated mice had reduced surface CD11b, known to be elevated upon monocyte activation in general and following postprandial hyperlipidemia (ref. 41 and Figure 4B). Extending evidence that monocyte activation was reduced, surface CD62L, which is expressed only on the Ly-6C^{hi} monocyte subset (42) and which is shed upon activation, was more abundant on the plasma membrane of Ly-6C^{hi} monocytes after apoE complementation (Figure 4C). Lipid loading of monocytes in the plasma may also have been modulated, because the increased side scatter associated with lipid uptake into circulating Ly-6C^{lo} CD11c^{+} monocytes (43), which preferentially express scavenger receptors and lipid response pathways (44), was reversed by apoE complementation (Figure 4, D and E). Ly-6C^{lo} monocytes also expressed less CD115 (CSF-1 receptor), a growth factor receptor for CSF-1 known to promote atherosclerosis (45), after apoE complementation (Figure 4F).

For quantification of monocyte recruitment into plaques by labeling monocyte subsets in vivo using the bead-labeling approach, monocyte subsets were labeled 1, 2, or 4 weeks after adenoviral treatment, and plaques were harvested for quantification from 1 to 5 days later, during the major period of monocyte entry (9). This experimental design was such that the bead-labeling assay could be used to monitor monocyte entry into plaques rather than their persistence, as in the experiments presented in Figure 3. Importantly, we verified that adenoviral infection did not affect the bead-labeling efficiency of blood monocytes and that the same number of monocytes was labeled in each group (data not shown). Quantification of monocyte recruitment into plaques after infection with the control adenoviral ad-Empty vector revealed that it slightly but non-significantly increased monocyte recruitment into plaques 1 week after infection, and this effect did not persist up to 2 weeks following infection (Figure 5A). To compile results from independent experiments, we compared the relative magnitude of monocyte subset entry into plaques between ad-hApoE3–treated mice and ad-Empty vector–treated mice. By 2 weeks after ad-hApoE3 vector treatment and thereafter, we observed a dramatic inhibition of both nonclassical (Figure 5B) and classical monocyte subset entry

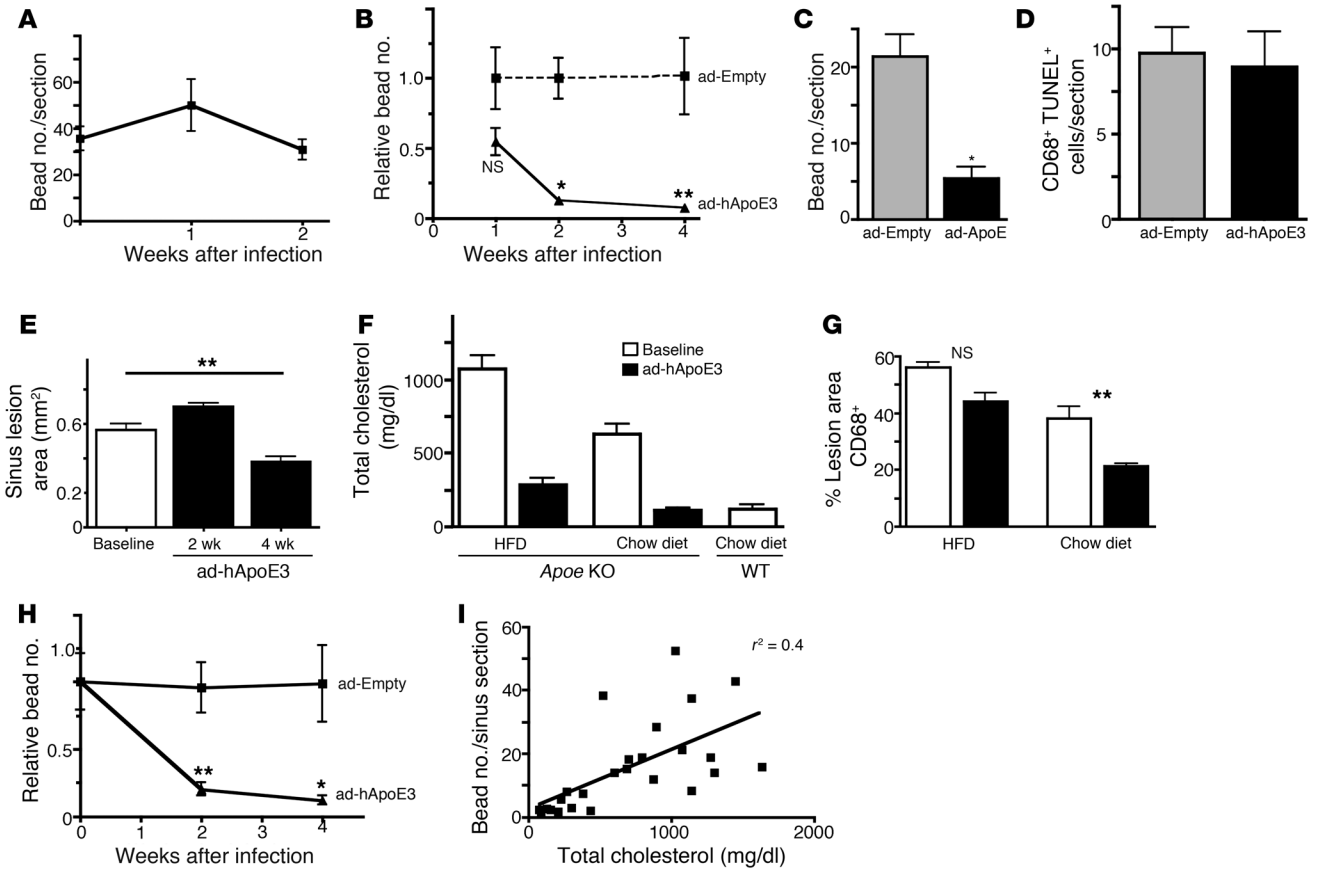

Figure 5

Monocyte recruitment and apoptotic death during macrophage loss from plaques. (**A**) Effect of ad-Empty vector infection on Ly-6C^{lo} monocyte recruitment into the plaque using the bead labeling assay. n = 5–7 mice/group. (**B**) Recruitment of Ly-6C^{lo} monocytes was quantified 1, 2, and 4 weeks (10, 11, and 13 weeks of HFD) after ad-hApoE3 infection and ad-Empty infection. Monocytes were labeled 2–6 days before sacrifice, depending on the experiment. Relative bead number was obtained by dividing the number of beads for each mouse by the number of beads averaged from the corresponding control ad-Empty group. Data represent 4 experiments; n = 5–7 mice per group. (**C**) Recruitment of Ly-6C^{hi} monocytes was quantified 2 weeks after ad-hApoE3 infection and ad-Empty infection. n = 5–7 mice/group. (**D**) Quantification of the number of CD68$^+$ TUNEL$^+$ DAPI$^+$ cells per section in the aortic sinus, 2 weeks after ad-Empty or ad-hApoE3 infection (n = 3–7/group). (**E**) Lesion area of chow-fed *Apoe*$^{-/-}$ mice, with baseline group analysis conducted at 31 weeks of age and further analysis 2 or 4 weeks after ad-hApoE3 vector infection; n = 5 mice per group. (**F**) Total plasma cholesterol in 17-week-old *Apoe*$^{-/-}$ mice fed a HFD, 31-week-old *Apoe*$^{-/-}$ mice fed a chow diet, and WT mice fed a chow diet (white bars). Additional measurements were made 2 weeks after ah-hApoE3 infection (black bars); n = 5 per group. (**G**) Fraction of lesion area, from *Apoe*$^{-/-}$ animals in **F**, containing CD68$^+$ cells. (**H**) Relative effect of ad-hApoE3 in altering monocyte recruitment in chow-fed *Apoe*$^{-/-}$ mice, using same approach as in **B** for HFD-fed *Apoe*$^{-/-}$ mice. (**I**) Correlation between total plasma cholesterol and monocyte recruitment measured after bead labeling of blood monocytes. Correlation is significant; $P < 0.001$. Data in all panels represent mean ± SEM; *$P < 0.01$; **$P < 0.001$.

(Figure 5C) into the plaque. Inhibition of monocyte recruitment into plaques appeared somewhat delayed relative to the kinetics of cholesterol lowering in plasma, since apoE complementation non-significantly reduced monocyte recruitment to plaques at 1 week after infection with ad-hApoE3 vector (Figure 5B).

In order for impaired monocyte recruitment to result in macrophage loss from plaques, there must also be a loss of macrophages due to turnover. We thus assessed whether apoE complementation altered apoptosis of plaque macrophages by quantifying the number of plaque cells that were CD68$^+$, DAPI$^+$, and TUNEL$^+$ per section, 2 weeks after ad-Empty or ad-hApoE3 vector treatment (Figure 5D). The vast majority of the DAPI$^+$ TUNEL$^+$ cells costained for CD68$^+$ (data not shown). Our analysis found a similar rate of macrophage apoptosis in plaques treated with ad-hApoE3 or ad-Empty (Figure 5D), indicating that an enhanced burst of apoptosis did not contribute to macrophage loss within *Apoe*$^{-/-}$ plaques after treatment of these mice with apoE-complementing virus. Instead, a stable rate of apoptosis coupled with a markedly reduced new supply of incoming monocytes served to reduce macrophage content in plaques over time. It is possible that macrophage content may also be influenced by changes in proliferation, but an analysis of Ki67 staining to assess this question revealed that the vast majority of proliferation in the plaques we examined was observed within α-actin$^+$ smooth muscle cells, whose rate of proliferation nearly doubled in response to apoE complementation (data not shown).

To lend support for the importance of monocyte recruitment in maintaining macrophage content of established plaques, we compared macrophage area in *Apoe*$^{-/-}$ plaques treated for 3 weeks

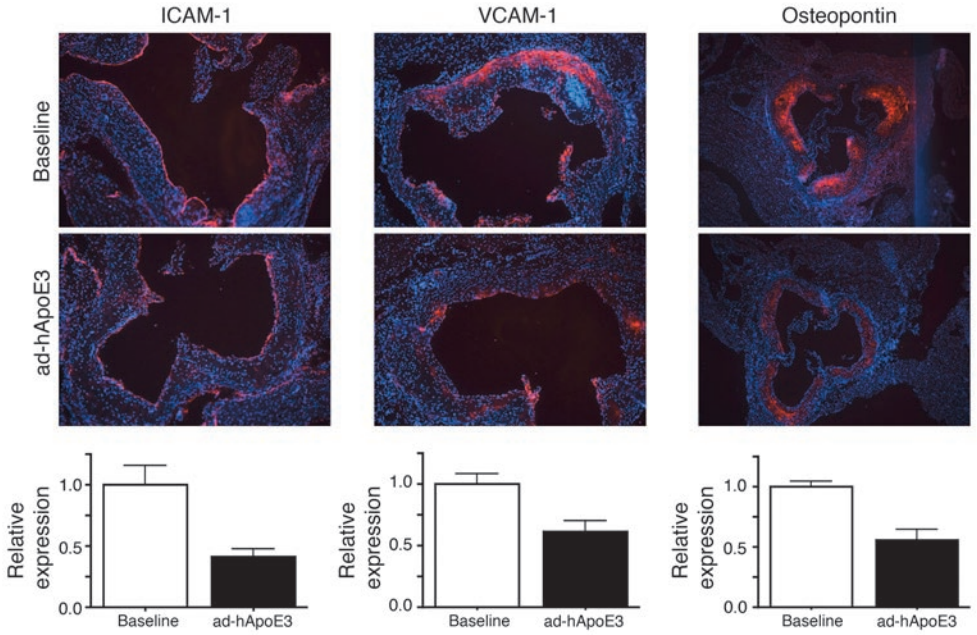

Figure 6
Effect of apoE complementation on the expression of adhesion molecules in atherosclerotic plaque. Immunofluorescent staining of ICAM-1, VCAM-1, and osteopontin (red) in aortic sinus lesions was carried out and quantified. Blue, nuclei. Original magnification, ×100 for ICAM-1 and VCAM-1, and ×50 for osteopontin. Quantifications of red area in a series of sections in 5 animals per stain are shown below each representative micrograph. All reductions in staining intensity of adhesion molecules were statistically significant, with a *P* value of 0.01 or less.

with biologically active pertussis toxin (PTX), an inhibitor of α_i-type G protein–coupled receptors that regulate the responsiveness of most chemoattractant receptors, versus those treated with PTX denatured by boiling. While systemic treatment with PTX no doubt has multiple effects, including induction of leukocytosis, we reasoned that its use would allow us to confirm that blocking monocyte entry into plaques would be associated with a reduction in plaque macrophage accumulation, independently of aggressively lowering cholesterol. Using a model of skin contact sensitization (46), we first verified that a single i.p. injection of PTX (2.5 μg/mouse), but not boiled PTX or PBS, efficiently impaired skin dendritic cell migration to lymph nodes (data not shown). Just prior to the end of a 3-week period of PTX treatment in HFD-fed *Apoe*$^{-/-}$ mice, circulating monocytes were bead labeled. Treatment with PTX partially inhibited monocyte recruitment into plaque (Supplemental Figure 5A) and decreased CD68$^+$ macrophage content by approximately one-half (Supplemental Figure 5B), with smaller changes in lesion area and ORO content (Supplemental Figure 5, C and D). PTX-treated mice showed a similar percentage of TUNEL$^+$ cells per plaque section (data not shown). These data further support the concept that targeting monocyte recruitment in established advanced plaques is a viable strategy for lowering plaque macrophage burden.

Next, we carried out a series of experiments in *Apoe*$^{-/-}$ mice fed a standard chow diet to discern whether apoE complementation under conditions of less extreme hypercholesterolemia led to a similar reduction in monocyte recruitment. We studied 31-week-old *Apoe*$^{-/-}$ mice fed a standard chow diet, as these older-age chow-fed *Apoe*$^{-/-}$ mice had lesion size similar to that in the HFD-fed younger *Apoe*$^{-/-}$ mice we studied (Figure 5E), while baseline cholesterol levels were approximately one-half those of the HFD-fed cohort (Figure 5F). The rise in cholesterol following its nadir in HFD-fed *Apoe*$^{-/-}$ mice (Figure 1A) was less apparent in the chow-fed animals, wherein cholesterol levels still hovered near *Apoe*$^{+/+}$ levels 2 weeks after apoE complementation (Figure 5F). Within 4 weeks following apoE complementation in the chow-fed *Apoe*$^{-/-}$ mice, lesion area was decreased (Figure 5E), in contrast to HFD-fed mice (Figure 1, B and C), consistent with earlier work (28). Macrophage area reductions in chow-fed *Apoe*$^{-/-}$ mice were significant 2 weeks after apoE complementation (Figure 5G). None of these differences were sufficient to lead to migratory egress from plaques, as assessed using the bead-labeling method (data not shown), but monocyte recruitment to plaques was dramatically reduced (Figure 5H) to an extent similar to that observed in the HFD-fed mice (Figure 5B). Indeed, these studies in chow-fed animals with or without apoE complementation extended the range of plasma cholesterol variations under which we quantified monocyte recruitment. Total plasma cholesterol and the magnitude of monocyte recruitment to plaque were positively correlated (Figure 5I), consistent with the concept that disease reversal characterized by aggressive cholesterol lowering is pivotally regulated by modulation of the recruitment of monocytes to plaque.

Understanding the complete mechanism behind suppression of monocyte recruitment in the context of apoE complementation is beyond the scope of this study. However, we did observe reduced expression of ICAM-1, VCAM-1, and osteopontin, molecules involved in the recruitment of monocytes across the arterial endothelium, in plaque sections 2 weeks after ad-hApoE3 vector treatment (Figure 6). Thus, apoE complementation leads to changes both within plaque (Figure 6) and within circulating monocytes (from Figure 5) that could, especially collectively, strongly suppress monocyte recruitment.

Discussion

To design therapies to reduce macrophage burden in atherosclerotic plaques, understanding of the cellular processes that regulate macrophage accumulation in atherosclerotic lesions is required, but the fundamental processes underlying removal of macrophages have not been determined. In the past years, the concept that migratory egress from plaques is a key feature of plaque regression has gained momentum (24–26, 36). However, due to lack of availability of quantitative approaches, past studies on egress have

generally not been quantitative and have examined migratory egress from plaques with little comparison to other processes that might reduce macrophage burden in plaques. Methods to quantify the migration of monocytes into atherosclerotic plaques have only recently been developed (8, 9). Here we show that one of these methods, the bead-tracking method we developed previously (9), permits quantitative assessment of not only monocyte entry into, but also their exit from, plaques (24–26, 36). By using this method, we investigated the relative importance of changes in the rate of monocyte entry versus egress from plaques in reducing macrophage burden after lowering of plasma total cholesterol, increasing HDL, and restoring apoE expression in *Apoe*$^{-/-}$ mice (9, 26, 28). Following adenoviral vector–mediated apoE complementation in *Apoe*$^{-/-}$ mice, we observed that removal of macrophages from plaques was strongly correlated with robustly reduced monocyte entry into plaques, coupled with a steady rate of apoptotic turnover, whereas migratory egress from plaques was minimal.

The concept of blocking monocyte entry into plaques as a therapy is not new (20). Indeed, it has been obvious that blocking influx of monocytes would prevent the expansion of macrophage area during plaque growth. However, our findings indicate that inhibiting monocyte influx does not simply stabilize, but instead actually reduces, macrophage content in plaques. Contrasting with our conclusion, for example, is a study by Guo et al. wherein bone marrow deficient in CCR2 was transplanted into irradiated *Apoe*$^{-/-}$ mice with developed plaques (47). Loss of macrophage content was not evident in these plaques (47), even though circulating monocytes would lack CCR2, leading the authors to conclude that suppressing monocyte entry into developed plaques was inconsequential for macrophage removal. Given our findings, the work of Guo et al. requires reinterpretation. For instance, it may be necessary to inhibit receptors other than, or in addition to, CCR2 to achieve macrophage loss from plaques, consistent with findings that several chemokine receptors are involved in monocyte accumulation within atherosclerotic plaques (9, 10, 48). Mice lacking CCR2, however, also have a marked deficiency in classical Ly-6C^{hi} monocytes in the blood (39, 49) due to a role for CCR2 in egress of monocytes from the bone marrow (49, 50), and it is this subset of monocytes that enters plaques of the aorta in a quantitatively dominant manner (9, 40). Thus, the mice studied by Guo et al. would also have had greatly reduced circulating Ly-6C^{hi} monocytes. It is interesting to note that the analysis of lesions in that study focused on the aortic root. In the present study, we were surprised to find that entry of labeled monocytes into aortic root plaques is far more robust than in the lesser curvature of the aortic arch, and that CCR2-negative Ly-6C^{lo} monocytes are as efficient at entering aortic root plaque as the Ly-6C^{hi} monocytes, quite distinct from the dominance of Ly-6C^{hi} monocytes in the lesser curvature (9, 40). That the two major subsets of monocytes appear to have different abilities to enter plaques in different regions of the arterial tree may explain why different plaques have distinct patterns of dependency on different homing molecules (51), possibly including CCR2 (47), which is not expressed on Ly-6C^{lo} monocytes. In any case, our findings underscore the concept that blocking monocyte entry into developed plaques has the potential to promote favorable changes in plaques, including reduction in macrophage burden. Blocking more than one receptor may be necessary, and more than one subset of monocytes may be relevant, especially in certain lesion sites.

Indeed, targeting inhibition of monocyte entry into plaques may be more likely to achieve success in removing macrophages than attempting to coax macrophages out of plaques by promoting their migratory egress. As our earlier studies using the surgical model of regression were not quantitative and included analysis of the whole aorta and not just the intima (24, 25), we combined the quantitative bead tracking approach with the surgical model and revealed that migratory egress from the intima is quantitatively significant. In contrast to the surgical model, two lines of evidence failed to support involvement of cell egress in the model of regression achieved in *Apoe*$^{-/-}$ mice by apoE complementation: (a) lack of a role for CCR7, proposed to mediate migratory egress through lymphatics (25), and (b) failure to observe quantitatively measurable egress using the bead-tracking model. A major difference between the surgical and apoE complementation models is that regression is much faster in the surgical model (24) than in the apoE complementation model (28). The slower process of reducing plaque macrophage content using apoE complementation in *Apoe*$^{-/-}$ mice likely more closely resembles therapeutic scenarios in humans (52).

The explanation for the mechanistic differences between the two regression models is not completely clear. Perhaps surgical intervention itself affects cellular behavior in plaques, as we have noticed more infiltration of the media by leukocytes in the surgical model, suggesting unusual breach of medial immunoprivilege (53, 54) accompanied by overwhelming adventitial inflammation (G.J. Randolph, unpublished observations). Based on the data in the present study, it seems reasonable to suppose that the pathway involving migratory egress from plaques is operative only in the context of certain stimuli not present in the apoE complementation model (e.g., breach of immunoprivilege). By contrast, the slower pathway of macrophage removal that we describe here — involving no or minimal induction of egress but stemming from a combination of reduction in signals to recruit monocytes and ongoing apoptosis of monocyte-derived cells within plaque — acts as a default means for regulating plaque macrophage content. Even though migratory egress in the surgical model of regression appears to rely on CCR7 and its ligands (25, 55), it would be unlikely that failure to express CCR7 would govern regression even in the surgical model, because the slower process of reducing macrophage burden that we describe here would be expected to take over, rendering the CCR7 pathway ultimately, if not immediately, dispensable. Indeed, we found that CCR7 was not required to lower macrophage accumulation in plaques of *Apoe*$^{-/-}$ mice treated with viral vectors encoding apoE, and its previously reported role in other models has not been explored beyond the first several days after induction of regression (55). Even if one would raise the unlikely possibility that adenoviral vectors encoding apoE may kick off a process that inhibits migratory egress, our data clearly reveal that macrophage burden in plaques can still be robustly decreased through suppression of monocyte entry, thus revealing that migratory egress is not essential during plaque regression to relieve macrophage burden.

With this study bringing focus on monocyte recruitment rather than egress as a means to reduce macrophage burden in plaques, the important next step will be to identify the molecular mechanisms that trigger and ultimately account for reduced monocyte recruitment. It seems logical that the attenuation of monocyte recruitment would be downstream of a critical shift in lipid composition in the plaque, and indeed we observed a marked decrease in cholesterol ester content within plaques. Plasma HDL levels increased robustly after apoE complementation, and the time course suggested that plasma HDL particles were especially heavily

laden with cholesterol on day 7. However, considering the mass spectroscopy data from aortae, it is unclear how much of this cholesterol originates from plaques within the first 2 weeks after apoE complementation. Nonetheless, the changes that occurred within plaques within this time frame led to a striking diminution in the inflammatory status of lesions, particularly evident in the strong blockade in recruitment of new monocytes. With regard to cholesterol mass measurements, our findings are reminiscent of previously published studies on monkeys, wherein the first period of regression, a period that included massive reduction in plaque macrophage content, was characterized by retention of cholesterol mass in plaques, with robust de-esterification of cholesterol leading to a relative increase in free cholesterol within lesions (56). As more time passed, cholesterol itself was cleared from plaques (56). In our study, we noted that the state of monocyte activation in the circulation was reduced and the expression of various adhesion receptors (ICAM-1, VCAM-1, etc.) was also decreased in lesions. These changes may account for the suppression of monocyte entry into plaques. It will be interesting in the future to determine how these changes come about in plaques and in particular whether and how they are linked to the mobilization of cholesterol from an esterified pool.

In humans, it has been shown that for every 1% reduction in LDL-C levels, relative risk for major coronary events is reduced by approximately 1% (52). The positive correlation we observed between the decrease in circulating total cholesterol, the decrease in cholesterol ester within plaque, and the reduction in monocyte recruitment to plaque is consistent with this observation in humans and the concept that foam cell content in plaque is a major independent risk factor for cardiovascular events. The data generated in this study support the idea that interfering with monocyte recruitment into plaques may be therapeutically beneficial, though it is also clear that such an approach should be carried out as ancillary therapy with aggressive lipid lowering in order to maintain and reinforce reductions in monocyte recruitment. Indeed, blocking monocyte entry into plaques as an add-on therapy to accompany aggressive lipid lowering may be a particular efficacious strategy to achieve further clinical advances in reducing rupture of vulnerable plaque that stems from activation of plaque macrophages.

Methods

Mice and adenoviral infection. Male and female C57BL/6J *Apoe*$^{-/-}$ mice expressing Ly5.1 (CD45.2) were purchased from the Jackson Laboratory, and *Apoe*$^{-/-}$ mice expressing Ly5.2 (CD45.1) were generated (24) and maintained in our colony. For each experiment, mice in all groups were matched according to their age, sex, and CD45 congenic marker (CD45.2 or CD45.1) status. *Ccr7*$^{-/-}$ (CD45.2^{+}) mice were purchased from the Jackson Laboratory (strain B6.129P2-Ccr7^{tm1Dgen}/J; stock 005794) and crossed to *Apoe*$^{-/-}$ (CD45.1^{+}) mice to generate *Apoe*$^{-/-}$*Ccr7*$^{-/-}$ mice. Littermate controls (*Apoe*$^{-/-}$*Ccr7*$^{+/+}$) were generated at the same time. Mice were housed in a specific pathogen–free environment and used in accordance with protocols approved by the Institutional Animal Care and Utilization Committee at Mount Sinai School of Medicine.

At the age of 5–6 weeks, mice were transitioned to a HFD (21% milk fat, 0.15% cholesterol; Harlan Teklad). Matched mice were divided into 3 groups. One group was sacrificed to establish baseline parameters in the plaque. The two other groups remained on a HFD for the duration of treatment and were infected either with apoE-encoding adenoviral vector (ad-hApoE3) or with its control empty adenoviral vector (ad-Empty) i.v. Infection was routinely verified in each animal by measuring total cholesterol levels after submandibular blood puncture. Total cholesterol levels were determined using a Wako kit (catalog 439-17501) according to the manufacturer's protocol. Lipoprotein cholesterol distributions were determined using thawed plasma samples diluted 1:1 in cold PBS centrifuged at 10,000 *g* for 2 minutes at 4°C. Approximately 15 mg of cholesterol was injected onto an HPLC system with online mixing of enzymatic reagent (Cholesterol Liquid Reagent Set, Pointe Scientific Inc.) with effluent from the column. The HPLC system consisted of a Superose 6 10/300 GL column (GE Healthcare); a LaChrom Elite HPLC system (Hitachi High Technologies) consisting of an L-2200 Autosampler with Peltier cooling, an L-2420 UV-Vis Detector, and two L-2100 SMASH pumps — one for delivering 0.9% saline with 0.01% EDTA and 0.01% sodium azide at 0.4 ml/min to the column and the other for delivering cholesterol reagent (or water) at 0.125 ml/min; a 5 m (length) × 0.5 mm (internal diameter) knitted reaction coil (KRC 5-50, Aura Industries Inc.) in a water jacket (CJB-10, Aura Industries Inc.) at 37°C; an Isotemp circulating water bath (Fisher Scientific); a PEEK Tee (Upchurch part no. P-712) at the junction of column effluent and total cholesterol reagent; and a personal computer running ChromPerfect Spirit Chromatography Data System, version 5.5 (Justice Laboratory Software) for data acquisition and analysis. Infected mice were sacrificed 1–6 weeks after infection.

Monocyte labeling in vivo. Nonclassical Ly-6C^{lo} monocytes were labeled in vivo by retro-orbital i.v. injection of 1 μm Fluoresbrite green fluorescent (YG) plain microspheres (Polysciences Inc.) diluted 1:4 in sterile PBS. Classical Ly-6C^{hi} monocytes were labeled with beads using the same protocol, but with beads administered 3 days after i.v. injection of 250 μl clodronate-loaded liposomes. Clodronate was a gift from Roche and was incorporated into liposomes as described previously (57). Labeling efficiency was verified by flow cytometry 1 day after labeling.

Surgical transfer of the aortic arch. Surgical transfer was performed as previously described (58). Briefly, 12 female *Apoe*$^{-/-}$ (CD45.1^{+}) mice were used at the age of 9 months. Three days before surgery, Ly-6C^{lo} monocytes were labeled with beads, as described above. Aortic arches were transplanted into female WT retired breeders (*Apoe*$^{+/+}$, CD45.2^{+}) that were matched in weight.

Analysis of atherosclerotic plaques. Mice were sacrificed and perfused with 10 ml PBS containing 2% EDTA. The heart and aorta were removed and fixed in 4% paraformaldehyde for 2 hours. The heart was transferred into PBS containing 30% sucrose (wt/vol) overnight at 4°C before being embedded in OCT compound and stored at –80°C. Cryosections (8 μm thickness) of the aortic sinus were prepared. Aortic arches were either likewise frozen in OCT compound and cross-sectioned (6 μm) or were opened en face for analysis. ORO (Sigma-Aldrich O-0625) staining was used to detect neutral lipids in the plaque. Sirius red staining was used to analyze collagen content. Plaque macrophages were analyzed by staining with anti-CD68 mAb (AbD Serotec MCA1957), anti–MOMA-2 mAb (AbD Serotec MCA519G), anti-F4/80 mAb (AbD Serotec MCA497BB), anti-Ki67 mAb, and/or anti-CD11c mAb (BD Biosciences — Pharmingen 553800). Vascular wall adhesion molecules were examined by staining with anti–ICAM-1 (BD Biosciences — Pharmingen 550287), anti–VCAM-1 (BD Biosciences — Pharmingen 550547), and anti-osteopontin (R&D Systems AF808) antibodies. Anti-rat or anti-hamster Cy3- or Cy5-conjugated antibodies were used for detection (Jackson ImmunoResearch Laboratories Inc.). Smooth muscle cells were identified by staining with anti–α-actin mAb (Sigma-Aldrich C6198). Nuclei were revealed with DAPI (5 μg/ml in mounting medium). TUNEL staining was carried out using the TMR red kit (Roche 12156792910). Quantification of plaque area and area occupied by a particular stain was calculated with ImageJ software. Beads in plaques were counted manually by fluorescence microscopy (9).

Cholesterol analysis. Lipids were extracted from aortic tissue according to Bligh and Dyer (59), with addition of 4 μg of [3,4-$^{14}C_2$]cholesterol as

the internal standard for cholesterol analyses. After evaporation under a stream of argon, the lipid extracts were dissolved in 1 ml chloroform/methanol (at 1:1) and stored at –80°C until analysis. An aliquot from each extract was evaporated under argon, dissolved in toluene, and then analyzed on a Thermo Fisher Trace 2000 mass spectrometer. One microliter of the reconstituted sample was injected in the splitless mode onto a 30 m × 250 μm DB-1 column (J&W Scientific) having a 0.25-μm film thickness. Helium carrier gas was set at 2 ml/min. The temperature program was as follows: 150°C for 1 minute, 150°C to 280°C at 25°C/min, ending at 280°C for 23 minutes. The samples were analyzed using positive ion–electron impact with selected ion monitoring (SIM) of *m/z* 386.4 for cholesterol and *m/z* 388.4 for [3,4-$^{13}C_2$]cholesterol. A second 50-μl aliquot was saponified at room temperature for 2 hours with methanolic-KOH, similar to a procedure using ethanol (60), cooled, and then extracted with hexane. After evaporation under argon, the residue was dissolved in 20 μl of toluene and analyzed for cholesterol content. Cholesteryl ester was calculated as the difference between the total cholesterol and free cholesterol values. All analyses were performed in glass vessels. A standard curve was prepared for quantitation. Aortic protein was determined by the Lowry method (61) using bovine serum albumin as the standard.

Flow cytometry. Mouse blood was collected by non-terminal submandibular or terminal cardiac puncture. Total leukocytes were quantitated by fresh blood dilution in Turk's solution (RICCA Chemical Company 8850-16). After red blood cell lysis (BD PharmLyse), monocyte subsets were identified by staining with anti-CD115 mAb (eBiosciences clone AFS98), CD11b (eBiosciences clone M1/70), CD11c (eBiosciences clone N418), and anti-Gr1/Ly-6C antibody (BioLegend, clone RB6-8C5). Data were acquired on a BD FACSCanto Flow Cytometer or a BD LSRII Flow Cytometer and analyzed with FlowJo software (Tree Star).

PTX treatment. C57BL/6 male mice were treated by i.p. injection of 2.5 μg PTX or 2.5 μg boiled PTX to inactivate the toxin but retain the ability to assess effects of heat-resistant endotoxin contamination. Contact hypersensitization assays (FITC painting) confirmed that this dose of PTX was sufficient to reduce dendritic cell migration to lymph nodes (46) for at least 5 days. In separate studies, 18-week HFD–fed female *Apoe*$^{-/-}$ mice were treated once weekly for 3 weeks with PTX (2.5 μg/mouse/wk) or control boiled PTX. Animals were subsequently sacrificed and arches and sinus analyzed as above.

Statistics. Data are expressed as mean ± SEM, except where otherwise indicated. Statistical differences were assessed using a 2-tailed *t* test or ANOVA (with Tukey's post-test analysis) with Prism software. A *P* value of less than 0.05 was considered statistically significant.

Acknowledgments

We thank Jianhua Liu (Mount Sinai School of Medicine), Manal Zabalawi, and Brian Fulp (Wake Forest University) for expert assistance. We thank Alan Tall, Molly Ingersoll, Andrew Platt, and Catherine Martel for critical reading of the manuscript. We thank the Department of Genetics and Genomic Science for assessment of the ALT measurement. Major support for this work includes NIH grants AI061741, AI049653, and HL096539 (subcontract to M.G. Sorci-Thomas), American Heart Association (AHA) Established Investigator Award 0740052, and a grant from the Experimental Therapeutics Institute, Mount Sinai Hospital to G.J. Randolph; NIH grants HL-49373 and HL-64163 to M.G Sorci-Thomas; and AHA grant 09GRNT2280053 and North Carolina Biotechnology Center grant 9903-IDG-1002 to M.J. Thomas. S. Potteaux was funded by Fondation pour la Recherche Medicale (France) and a 2007 Norman Alpert Visiting Scientist Award from the European Society of Cardiology/AHA. E.L. Gautier was funded by the AHA (10POST4160140).

Received for publication May 23, 2010, and accepted in revised form February 19, 2011.

Address correspondence to: Gwendalyn J. Randolph, Department of Gene and Cell Medicine, 1425 Madison Avenue, Box 1496, Room 13-02, Mount Sinai School of Medicine, New York, New York, USA. Phone: 212.659.8262; Fax: 212.803.6740; E-mail: gwendalyn.randolph@mssm.edu.

1. Glass CK, Witztum JL. Atherosclerosis: the road ahead. *Cell*. 2001;104(4):503–516.
2. Gautier EL, Jakubzick C, Randolph GJ. Regulation of the migration and survival of monocyte subsets by chemokine receptors and its relevance to atherosclerosis. *Arterioscler Thromb Vasc Biol*. 2009; 29(10):1412–1418.
3. Farb A, et al. Coronary plaque erosion without rupture into a lipid core. A frequent cause of coronary thrombosis in sudden coronary death. *Circulation*. 1996;93(7):1354–1363.
4. Shah PK. Pathophysiology of plaque rupture and the concept of plaque stabilization. *Cardiol Clin*. 1996;14(1):17–29.
5. Libby P, Schoenbeck U, Mach F, Selwyn AP, Ganz P. Current concepts in cardiovascular pathology: the role of LDL cholesterol in plaque rupture and stabilization. *Am J Med*. 1998;104(2A):14S–18S.
6. Yilmaz A, et al. Emergence of dendritic cells in rupture-prone regions of vulnerable carotid plaques. *Atherosclerosis*. 2004;176(1):101–110.
7. Virmani R, Burke AP, Farb A, Kolodgie FD. Pathology of the vulnerable plaque. *J Am Coll Cardiol*. 2006; 47(8 suppl):C13–C18.
8. Swirski FK, et al. Monocyte accumulation in mouse atherogenesis is progressive and proportional to extent of disease. *Proc Natl Acad Sci U S A*. 2006; 103(27):10340–10345.
9. Tacke F, et al. Monocyte subsets differentially employ CCR2, CCR5, and CX3CR1 to accumulate within atherosclerotic plaques. *J Clin Invest*. 2007; 117(1):185–194.
10. Combadiere C, et al. Combined inhibition of CCL2, CX3CR1, and CCR5 abrogates Ly6C(hi) and Ly6C(lo) monocytosis and almost abolishes atherosclerosis in hypercholesterolemic mice. *Circulation*. 2008;117(13):1649–1657.
11. Chapman CM, Beilby JP, McQuillan BM, Thompson PL, Hung J. Monocyte count, but not C-reactive protein or interleukin-6, is an independent risk marker for subclinical carotid atherosclerosis. *Stroke*. 2004;35(7):1619–1624.
12. Nasir K, Guallar E, Navas-Acien A, Criqui MH, Lima JA. Relationship of monocyte count and peripheral arterial disease: results from the National Health and Nutrition Examination Survey 1999-2002. *Arterioscler Thromb Vasc Biol*. 2005;25(9):1966–1971.
13. Johnsen SH, et al. Monocyte count is a predictor of novel plaque formation: a 7-year follow-up study of 2610 persons without carotid plaque at baseline the Tromso Study. *Stroke*. 2005;36(4):715–719.
14. Huang G, et al. Significance of white blood cell count and its subtypes in patients with acute coronary syndrome. *Eur J Clin Invest*. 2009;39(5):348–358.
15. Zhu SN, Chen M, Jongstra-Bilen J, Cybulsky MI. GM-CSF regulates intimal cell proliferation in nascent atherosclerotic lesions. *J Exp Med*. 2009; 206(10):2141–2149.
16. Fuster JJ, Fernandez P, Gonzalez-Navarro H, Silvestre C, Nabah YN, Andres V. Control of cell proliferation in atherosclerosis: insights from animal models and human studies. *Cardiovasc Res*. 2010;86(2):254–264.
17. Helgadottir A, et al. A common variant on chromosome 9p21 affects the risk of myocardial infarction. *Science*. 2007;316(5830):1491–1493.
18. McPherson R, et al. A common allele on chromosome 9 associated with coronary heart disease. *Science*. 2007;316(5830):1488–1491.
19. Visel A, et al. Targeted deletion of the 9p21 noncoding coronary artery disease risk interval in mice. *Nature*. 2010;464(7287):409–412.
20. Gautier EL, et al. Macrophage apoptosis exerts divergent effects on atherogenesis as a function of lesion stage. *Circulation*. 2009;119(13):1795–1804.
21. Tabas I. Macrophage death and defective inflammation resolution in atherosclerosis. *Nat Rev Immunol*. 2010;10(1):36–46.
22. Landsman L, et al. CX3CR1 is required for monocyte homeostasis and atherogenesis by promoting cell survival. *Blood*. 2009;113(4):963–972.
23. Bellingan GJ, Caldwell H, Howie SE, Dransfield I, Haslett C. In vivo fate of the inflammatory macrophage during the resolution of inflammation: inflammatory macrophages do not die locally, but emigrate to the draining lymph nodes. *J Immunol*. 1996;157(6):2577–2585.
24. Llodra J, Angeli V, Liu J, Trogan E, Fisher EA, Randolph GJ. Emigration of monocyte-derived cells from atherosclerotic lesions characterizes regressive, but not progressive, plaques. *Proc Natl Acad Sci U S A*. 2004;101(32):11779–11784.
25. Trogan E, et al. Gene expression changes in foam cells and the role of chemokine receptor CCR7 during

atherosclerosis regression in ApoE-deficient mice. *Proc Natl Acad Sci U S A*. 2006;103(10):3781–3786.
26. Williams KJ, Feig JE, Fisher EA. Rapid regression of atherosclerosis: insights from the clinical and experimental literature. *Nat Clin Pract Cardiovasc Med*. 2008;5(2):91–102.
27. Nagao T, Qin C, Grosheva I, Maxfield FR, Pierini LM. Elevated cholesterol levels in the plasma membranes of macrophages inhibit migration by disrupting RhoA regulation. *Arterioscler Thromb Vasc Biol*. 2007;27(7):1596–1602.
28. Tsukamoto K, Tangirala R, Chun SH, Pure E, Rader DJ. Rapid regression of atherosclerosis induced by liver-directed gene transfer of ApoE in ApoE-deficient mice. *Arterioscler Thromb Vasc Biol*. 1999; 19(9):2162–2170.
29. Zabalawi M, et al. Induction of fatal inflammation in LDL receptor and ApoA-I double-knockout mice fed dietary fat and cholesterol. *Am J Pathol*. 2003; 163(3):1201–1213.
30. Millar JS, et al. Short-term overexpression of DGAT1 or DGAT2 increases hepatic triglyceride but not VLDL triglyceride or apoB production. *J Lipid Res*. 2006; 47(10):2297–2305.
31. Nunnari JJ, Zand T, Joris I, Majno G. Quantitation of oil red O staining of the aorta in hypercholesterolemic rats. *Exp Mol Pathol*. 1989;51(1):1–8.
32. Förster R, et al. CCR7 coordinates the primary immune response by establishing functional microenvironments in secondary lymphoid organs. *Cell*. 1999; 99(1):23–33.
33. Ohl L, et al. CCR7 governs skin dendritic cell migration under inflammatory and steady-state conditions. *Immunity*. 2004;21(2):279–288.
34. Martin-Fontecha A, et al. Regulation of dendritic cell migration to the draining lymph node: impact on T lymphocyte traffic and priming. *J Exp Med*. 2003;198(4):615–621.
35. Tacke F, Ginhoux F, Jakubzick C, van Rooijen N, Merad M, Randolph GJ. Immature monocytes acquire antigens from other cells in the bone marrow and present them to T cells after maturing in the periphery. *J Exp Med*. 2006;203(3):583–597.
36. Randolph GJ. Emigration of monocyte-derived cells to lymph nodes during resolution of inflammation and its failure in atherosclerosis. *Curr Opin Lipidol*. 2008;19(5):462–468.
37. Angeli V, et al. B cell-driven lymphangiogenesis in inflamed lymph nodes enhances dendritic cell mobilization. *Immunity*. 2006;24(2):203–215.
38. Randolph GJ, Inaba K, Robbiani DF, Steinman RM, Muller WA. Differentiation of phagocytic monocytes into lymph node dendritic cells in vivo. *Immunity*. 1999;11(6):753–761.
39. Qu C, et al. Role of CCR8 and other chemokine pathways in the migration of monocyte-derived dendritic cells to lymph nodes. *J Exp Med*. 2004; 200(10):1231–1241.
40. Swirski FK, et al. Ly-6Chi monocytes dominate hypercholesterolemia-associated monocytosis and give rise to macrophages in atheromata. *J Clin Invest*. 2007;117(1):195–205.
41. van Oostrom AJ, et al. Activation of leukocytes by postprandial lipemia in healthy volunteers. *Atherosclerosis*. 2004;177(1):175–182.
42. Geissmann F, Jung S, Littman DR. Blood monocytes consist of two principal subsets with distinct migratory properties. *Immunity*. 2003;19(1):71–82.
43. Wu H, et al. Functional role of CD11c+ monocytes in atherogenesis associated with hypercholesterolemia. *Circulation*. 2009;119(20):2708–2717.
44. Ingersoll MA, et al. Comparison of gene expression profiles between human and mouse monocyte subsets. *Blood*. 2010;115(3):e10–19.
45. Shaposhnik Z, Wang X, Lusis AJ. Arterial colony stimulating factor-1 influences atherosclerotic lesions by regulating monocyte migration and apoptosis. *J Lipid Res*. 2010;51(7):1962–1970.
46. Robbiani DF, Finch RA, Jager D, Muller WA, Sartorelli AC, Randolph GJ. The leukotriene C(4) transporter MRP1 regulates CCL19 (MIP-3beta, ELC)-dependent mobilization of dendritic cells to lymph nodes. *Cell*. 2000;103(5):757–768.
47. Guo J, et al. Repopulation of apolipoprotein E knockout mice with CCR2-deficient bone marrow progenitor cells does not inhibit ongoing atherosclerotic lesion development. *Arterioscler Thromb Vasc Biol*. 2005;25(5):1014–1019.
48. Saederup N, Chan L, Lira SA, Charo IF. Fractalkine deficiency markedly reduces macrophage accumulation and atherosclerotic lesion formation in CCR2$^{-/-}$ mice: evidence for independent chemokine functions in atherogenesis. *Circulation*. 2008; 117(13):1642–1648.
49. Serbina NV, Pamer EG. Monocyte emigration from bone marrow during bacterial infection requires signals mediated by chemokine receptor CCR2. *Nat Immunol*. 2006;7(3):311–317.
50. Tsou CL, et al. Critical roles for CCR2 and MCP-3 in monocyte mobilization from bone marrow and recruitment to inflammatory sites. *J Clin Invest*. 2007; 117(4):902–909.
51. Teupser D, Pavlides S, Tan M, Gutierrez-Ramos JC, Kolbeck R, Breslow JL. Major reduction of atherosclerosis in fractalkine (CX3CL1)-deficient mice is at the brachiocephalic artery, not the aortic root. *Proc Natl Acad Sci U S A*. 2004;101(51):17795–17800.
52. Grundy SM, et al. Implications of recent clinical trials for the National Cholesterol Education Program Adult Treatment Panel III guidelines. *Circulation*. 2004;110(2):227–239.
53. Dal Canto AJ, Swanson PE, O'Guin AK, Speck SH, Virgin HW. IFN-gamma action in the media of the great elastic arteries, a novel immunoprivileged site. *J Clin Invest*. 2001;107(2):R15–R22.
54. Cuffy MC, et al. Induction of indoleamine 2,3-dioxygenase in vascular smooth muscle cells by interferon-gamma contributes to medial immunoprivilege. *J Immunol*. 2007;179(8):5246–5254.
55. Feig JE, et al. LXR is required for maximal egress of monocyte-derived cells from mouse aortic plaques during atherosclerosis regression. *J Clin Invest*. 2010; 120(12):4415–4424.
56. Small DM, Bond MG, Waugh D, Prack M, Sawyer JK. Physicochemical and histological changes in the arterial wall of nonhuman primates during progression and regression of atherosclerosis. *J Clin Invest*. 1984;73(6):1590–1605.
57. Van Rooijen N, Sanders A. Liposome mediated depletion of macrophages: mechanism of action, preparation of liposomes and applications. *J Immunol Methods*. 1994;174(1–2):83–93.
58. Chereshnev I, et al. Mouse model of heterotopic aortic arch transplantation. *J Surg Res*. 2003;111(2):171–176.
59. Bligh EG, Dyer WJ. A rapid method of total lipid extraction and purification. *Can J Biochem Physiol*. 1959;37(8):911–917.
60. Nordskog BK, Reagan JW Jr, St Clair RW. Sterol synthesis is up-regulated in cholesterol-loaded pigeon macrophages during induction of cholesterol efflux. *J Lipid Res*. 1999;40(10):1806–1817.
61. Lowry OH, Rosebrough NJ, Farr AL, Randall RJ. Protein measurement with the Folin phenol reagent. *J Biol Chem*. 1951;193(1):265–275.